Key Points:
- Whistler mode waves are observed on the magnetic reconnection separatrix
- These waves are propagating toward the X line
- Solitary bipolar parallel electric fields appear to be in phase with the wave and may correspond with electron enhancements

Correspondence to:
F. D. Wilder,
frederick.wilder@lasp.colorado.edu

Observations of whistler mode waves with nonlinear parallel electric fields near the dayside magnetic reconnection separatrix by the Magnetospheric Multiscale mission

F. D. Wilder[1], R. E. Ergun[1,2], K. A. Goodrich[1,2], M. V. Goldman[3], D. L. Newman[3], D. M. Malaspina[1], A. N. Jaynes[1], S. J. Schwartz[1,4], K. J. Trattner[1], J. L. Burch[5], M. R. Argall[6], R. B. Torbert[6], P.-A. Lindqvist[7], G. Marklund[7], O. Le Contel[8], L. Mirioni[8], Yu. V. Khotyaintsev[9], R. J. Strangeway[10], C. T. Russell[10], C. J. Pollock[10], B. L. Giles[10], F. Plaschke[11], W. Magnes[11], S. Eriksson[1], J. E. Stawarz[1,2], A. P. Sturner[1,2], and J. C. Holmes[1,2]

[1]Laboratory of Atmospheric and Space Physics, University of Colorado Boulder, Boulder, Colorado, USA, [2]Department of Astrophysical and Planetary Sciences, University of Colorado Boulder, Boulder, Colorado, USA, [3]Department of Physics, University of Colorado Boulder, Boulder, Colorado, USA, [4]Department of Physics, Imperial College London, London, UK, [5]Southwest Research Institute, San Antonio, Texas, USA, [6]Department of Physics, University of New Hampshire, Durham, New Hampshire, USA, [7]Royal Institute of Technology, Stockholm, Sweden, [8]Laboratoire de Physique des Plasmas, CNRS/Ecole Polytechnique/UPMC/P11, Vélizy, France, [9]Swedish Institute of Space Physics, Uppsala, Sweden, [10]Department of Earth, Planetary and Space Sciences, University of California, Los Angeles, California, USA, [11]Space Research Institute, Austrian Academy of Sciences, Graz, Austria

Abstract We show observations from the Magnetospheric Multiscale (MMS) mission of whistler mode waves in the Earth's low-latitude boundary layer (LLBL) during a magnetic reconnection event. The waves propagated obliquely to the magnetic field toward the X line and were confined to the edge of a southward jet in the LLBL. Bipolar parallel electric fields interpreted as electrostatic solitary waves (ESW) are observed intermittently and appear to be in phase with the parallel component of the whistler oscillations. The polarity of the ESWs suggests that if they propagate with the waves, they are electron enhancements as opposed to electron holes. The reduced electron distribution shows a shoulder in the distribution for parallel velocities between 17,000 and 22,000 km/s, which persisted during the interval when ESWs were observed, and is near the phase velocity of the whistlers. This shoulder can drive Langmuir waves, which were observed in the high-frequency parallel electric field data.

1. Introduction

Magnetic reconnection is a fundamental process in plasma physics. By converting stored magnetic energy into kinetic energy and heat, it drives large-scale plasma convection and allows for transport of energy from the solar wind into planetary magnetospheres [e.g., *Dungey*, 1961]. Although the introduction of Hall physics has led to improved understanding of the ion scale processes associated with magnetic reconnection, as well as improved prediction of reconnection rates [e.g., *Birn et al.*, 2001; *Mozer et al.*, 2008], the process is still not well understood at electron scales [*Burch and Drake*, 2009; *Hesse et al.*, 2011]. In particular, the interaction between magnetic reconnection and the local plasma populations warrants further investigation.

An example of these local interactions is plasma waves that are excited by, and interact with, the reconnection process. For example, whistler mode waves in the vicinity of the reconnection X-line have been observed during magnetopause crossings in the past and have been suggested to mediate the reconnection process [*Mandt et al.*, 1994; *Deng and Matsumoto*, 2001]. *Graham et al.* [2016] performed a statistical study of Cluster reconnection observations and found that whistler waves could propagate along the magnetic separatrix toward the X line. *Tang et al.* [2013] also found, using Time History of Events and Macroscale Interactions during Substorms (THEMIS) data, that whistler mode waves could propagate away from the electron diffusion region. Further, electrostatic solitary waves (ESWs) have been observed near the reconnection region, often at different time scales and speeds, suggesting that they can be generated by either a variety of different plasma instabilities or different regimes of the same instability [*Cattell et al.*, 2002; *Matsumoto et al.*, 2003; *Graham et al.*, 2015]. Numerical simulations also suggest that electron scattering by phase space holes

associated with ESWs are present near the X line and can contribute to electron heating near the reconnection site [*Drake et al.*, 2003; *Che et al.*, 2010].

Wave phenomena such as whistlers and ESWs can come from a variety of sources. In the magnetotail, whistler mode waves have been associated with perpendicular heating of few to tens of keV electrons in reconnection exhausts and dipolarization fronts, leading to a temperature anisotropy that promotes wave growth [e.g., *Wei et al.*, 2007; *Le Contel et al.*, 2009]. Temperature anisotropy due to betatron acceleration in the dipolarization front flux pileup region has also been observed to grow whistler mode waves [e.g., *Fujimoto and Sydora*, 2008; *Khotyaintsev et al.*, 2011; *Viberg et al.*, 2014]. Numerical simulations of reconnection have shown double layers on the reconnection separatrix, which can produce ESWs in the form of electron phase space holes [*Chen et al.*, 2015]; the Cluster mission observed these double layers on the separatrix during several magnetopause crossings [*Wang et al.*, 2014]. Buneman instabilities can also lead to the generation of ESWs [*Che et al.*, 2010]. Finally, recent simulations and theoretical studies have suggested that electron phase space holes can be produced on the separatrix by two-stream instabilities, which in turn can Cherenkov emit whistler mode waves [*Goldman et al.*, 2014]. Because of the multitude of different wave modes and possible generation mechanisms associated with reconnection, further study is necessary to understand the role of wave phenomena in this ubiquitous process.

In March 2015, NASA launched the Magnetospheric Multiscale (MMS) mission to study magnetic reconnection at electron scales. The mission includes four spacecraft in a tetrahedral formation, where each spacecraft measures electromagnetic field and particle data at unprecedented time resolution [*Burch et al.*, 2015]. In the present study, high-resolution burst mode data from this mission are used to investigate a dayside magnetopause reconnection event on 19 September 2015. During this event, oblique whistler waves and ESWs were observed in the vicinity of two reconnection exhaust reversals. DC-coupled electric and AC magnetic field data sampled at 8192 samples/second (S/s) from the electric field double probe instruments [*Ergun et al.*, 2014; *Lindqvist et al.*, 2014] and search coil magnetometer (SCM) [*Le Contel et al.*, 2014] are used to investigate the spectral and propagation characteristics of the whistler waves and ESWs. Additionally, 65,536 S/s AC-coupled electric field data were used to identify Langmuir oscillations in the vicinity of the whistler waves. Data from the Fast Plasma Instrument (FPI) [*Burch et al.*, 2015], electron drift instrument (EDI) [*Torbert et al.*, 2014], and flux gate magnetometer [*Russell et al.*, 2014] provide context for the waves with respect to the reconnection geometry. We show that the whistler mode waves are confined to the boundary layer and propagate along the magnetosphere-side separatrix of the X line. This observation suggests local generation of the whistler mode waves. Additionally, we show that the parallel electric fields associated with the whistler are spiky and that observed ESWs appear to be in phase with the whistler mode waves' parallel electric field oscillations.

2. Observations of the Magnetopause Crossing

2.1. Event Overview

Figures 1a–1j show an overview of data from MMS4 between ~10:03 and 10:10 UT on 19 September 2015 and Figure 1k shows a cartoon corresponding to the event. The magnetic field and ion bulk velocity are given in Geocentric Solar Ecliptic (GSE) coordinates. The Poynting flux is given in field-aligned coordinates and was evaluated using electric and magnetic field data filtered with a passband between 100 and 1000 Hz. The passband was chosen to remove the DC component of the electric field as well as oscillations above the waves of interest for the present study. The field-aligned coordinate (FAC) system is described as follows: Z (labeled $\parallel$) is parallel to the background field ($\mathbf{B}_0$) measured by the fluxgate magnetometer at the survey data rate (16 S/s), X (labeled P1) is perpendicular to $\mathbf{B}_0$ and in the spacecraft spin plane, and Y (labeled P2) completes the right-handed system.

Earlier in the interval, the spacecraft was in the magnetosheath, and at approximately 10:03:55, the north-south magnetic field component, B_Z, began to rotate from southward to northward with a positive enhancement in the ion bulk velocity V_Z component. At approximately 10:06 UT, V_Z turned sharply negative, reaching a minimum of -300 km/s, which is faster than the background magnetosheath flow which is approximately 180 km/s and is a signature of a reconnection exhaust [e.g., *Eriksson et al.*, 2004, and references therein]. *Trattner et al.* [2016] found "D"-shaped ion distributions during both the positive and negative V_Z enhancements, which are signatures of a reconnection exhaust. At 10:06:33 (indicated by the first vertical dashed line),
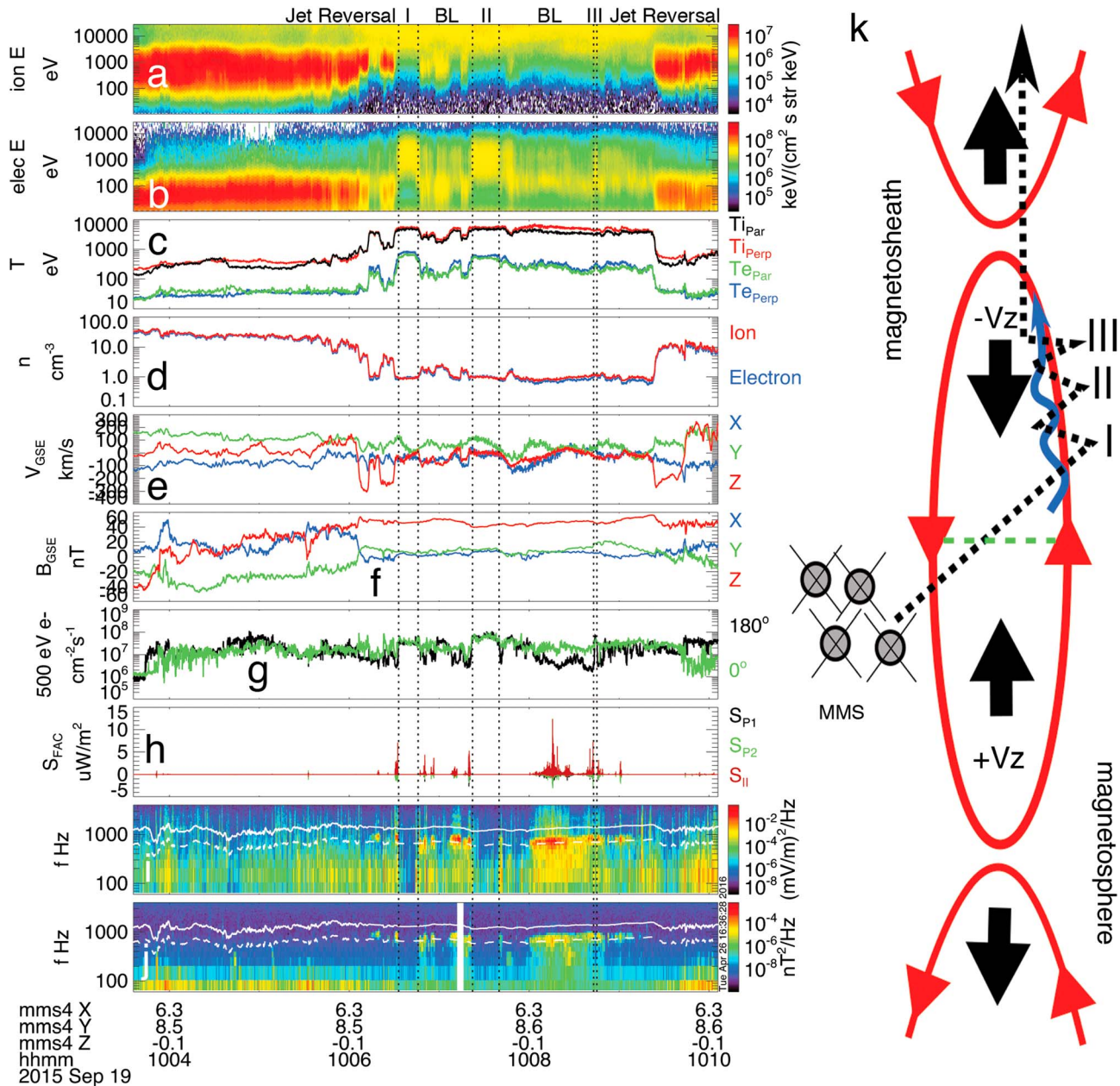
Figure 1. Overview of jet reversal crossing and separatrix skimming by MMS4 on 19 September 2015. (a) ion energy spectra, (b) electron energy spectra, (c) ion and electron temperatures, (d) ion and electron number density, (e) ion bulk velocity in GSE coordinates, (f) magnetic field vector in GSE coordinates, (g) ambient 500 eV electron flux at 0 and 180° pitch angle, (h) Poynting flux in FAC coordinates, (i) electric field, and (j) magnetic field power spectral density. Solid and dashed white lines indicate f_{ce} and $f_{ce}/2$. Vertical dashed lines indicate full crossings between the boundary layer and the magnetosphere as determined from the electron spectra and ambient electron counts. (k) Cartoon illustrating MMS trajectory. Red lines are magnetic field lines, black arrows are the exhausts, and wavy blue arrows are the whistler waves.

the V_z flow approached zero, and the ion density dropped to less than $1\,cm^{-3}$. Additionally, the electron temperature increased to 400 eV and the magnetic field vector components stabilized compared to earlier (the magnetosheath and low-latitude boundary layer), suggesting the spacecraft exited the boundary layer and fully entered the magnetosphere. Just before this first crossing, at the edge of the reconnection exhaust, EDI's ambient electron detector (500 eV) observed a jump in electron flux parallel to the magnetic field, followed by a jump in antiparallel flux. After this jump, parallel and antiparallel electrons are balanced, suggesting the crossing of the reconnection separatrix into the closed field line region, similar to what has been observed by THEMIS [Øieroset et al., 2015].

For the remainder of the interval, the spacecraft crossed in and out of the magnetosphere, with each full crossing shown by vertical solid dashed lines, and the full magnetospheric excursions labeled by the Roman numerals I, II, and III in both the time series figure and the cartoon. We note shortly after interval II, there may have been another brief excursion into the magnetosphere; however, the crossing is not as clear in the particle data. Due to fluctuating asymmetry between 0° and 180° electrons, it is likely that the spacecraft also skimmed the separatrix. At the end of the plotted interval, the spacecraft reentered the jet and observed another V_Z reversal from negative to positive, suggesting the crossing of either an X line or a magnetic island. *Trattner et al.* [2016] confirmed that these flow enhancements were also reconnection exhausts with the characteristic "D"-shaped ion distribution. The analysis by *Trattner et al.* [2016] also suggested that the region of maximum magnetic shear was above the spacecraft at the beginning of the interval and moved southward in response to a sudden northward turning of the interplanetary magnetic field. Timing analysis between the spacecraft is inconclusive, but if the southward motion of the X line implied by *Trattner et al.* [2016] occurs, the first flow reversal may be converging flow (a magnetic island), and the second reversal is diverging flow (an X line). This interpretation is shown in Figure 1k. An alternative explanation is that the X line moved upward and back down; however, the remainder of this study will be focused on the southward jet.

At the edge of the southward jet, wave trains are seen in the electric and magnetic field spectra near half the electron cyclotron frequency (f_{ce}). These waves are seen throughout the interval and, from Figure 1, appear to be confined to the boundary layer between the edge of the reconnection exhaust and the magnetosphere-side separatrix. The wave trains are seen on all four MMS spacecraft (not shown), which at this time were separated by approximately 60 km. Polarization analysis of magnetic field spectra [e.g., *Samson and Olson*, 1980; *Le Contel et al.*, 2009] show ellipticity of approximately 1 and a degree of polarization of 90% near $f_{ce}/2$. Additionally, from Figure 1h, the Poynting flux exhibits mostly positive $S_\parallel$ whenever there is enhanced wave power near $f_{ce}/2$, with smaller S_{P1} and S_{P2}. The angle between **S** and **B**$_0$ as measured by the fluxgate magnetometer (16 samples/s with ~8 Hz response) and which can range from 0 to 180° was approximately 20° for all wave trains. The propagation angle indicates the electromagnetic component of the waves consists of right-handed circularly polarized whistler mode waves propagating obliquely with respect to the background field [*Le Contel et al.*, 2009].

Although a few of the wave trains are above $f_{ce}/2$, several lie very near $f_{ce}/2$, which suggest that the spacecraft is near the source region of the waves according to the propagation and dispersion model of *Omura et al.* [2009]. Because the wave trains do not exist in the magnetosphere proper and are observed near $f_{ce}/2$, we conclude that the waves are produced by local plasma conditions, as opposed to being chorus waves propagating from the inner magnetosphere.

Figure 1k shows a cartoon summarizing the event. The spacecraft crosses the magnetopause, encountering the converging flow of a magnetic island. It then proceeds to skim the separatrix, fully crossing into the magnetosphere three times, marked with the roman numerals I, II, and III corresponding to Figure 1a. At the separatrix, the spacecraft encounters whistler waves, represented by the blue arrow, propagating approximately along the magnetic field toward the X line. Whistlers have been observed in the past near the reconnection separatrix, with the waves tending to propagate toward the X line on the magnetospheric side [*Graham et al.*, 2016].

2.2. Whistler Wave Train and Bipolar Parallel Electric Fields

In the vicinity of the whistler mode waves, the electric field spectrum in Figure 1i shows lower amplitude broadband electrostatic activity, while the magnetic field spectrum is confined to a band near $f_{ce}/2$. Additionally, oscillations at harmonics of $f_{ce}/2$ are seen in the electric field spectra, but not in the magnetic field spectra. These spectral characteristics suggest a nonlinear kinetic interaction between the electric field and the local plasma populations. These interactions can include trapping of electrons by the electrostatic portion of oblique whistlers along the wave vector direction [*Kellogg et al.*, 2010]. The 8192 S/s electric and magnetic field data on MMS provide an opportunity to study these nonlinear reactions in detail. Figure 2a shows the electric and magnetic field power spectra, as well as the DC-coupled electric field in field-aligned coordinates. The time series in Figure 2c, shown in yellow, is a weighted average of residuals removed from the axial electric field measurement associated with spacecraft charging, the presence of cold plasma, and harmonics of the spin tone. The residual error applies to the frequency band from DC to 2 Hz. The sensitivity at 1 kHz is ~25 μV/m [*Ergun et al.*, 2014].
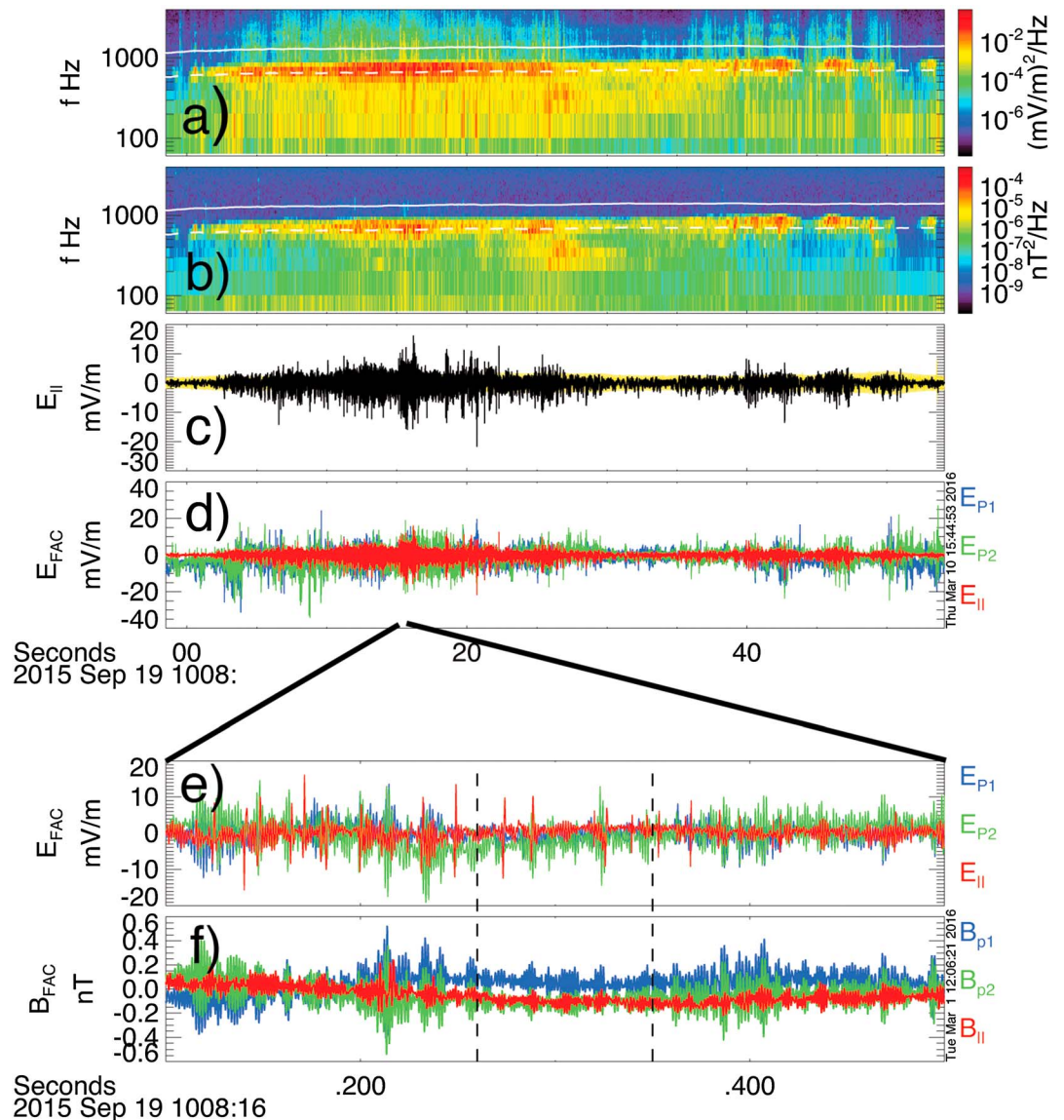
Figure 2. MMS4 electric and magnetic field data during the longest whistler wave train. (a) Electric field power spectral density, (b) magnetic field power spectral density, (c) parallel electric field, and (d) the electric field vector in field-aligned coordinates. Yellow indicates uncertainty in the DC parallel electric field. Additionally, 500 ms of the (e) electric and (f) magnetic field vectors in field-aligned coordinates beginning at 10:08:16 UT are shown. Vertical dashed lines indicate the times for which reduced electron distributions are shown in Figure 3.

Several nonlinear features are immediately apparent from Figure 2. These include a negative bias in $E_\parallel$, with negative spikes exceeding -10 mV/m and in one case exceeding -20 mV/m. Spiky nonlinear parallel components of whistler waves have also been observed in the Earth's radiation belts [*Mozer et al.*, 2014]. Additionally, broadband features in the electric field spectrum are seen throughout the interval when there is significant wave power at $f_{ce}/2$. Broadband electric field spectra are often associated with transient electric field structures such as electrostatic solitary waves (ESWs) [e.g., *Ergun et al.*, 1998a, 1998b]. Figures 2e and 2f show a zoomed in time series of the electric and magnetic field in field-aligned coordinates during an interval where significant broadband electric field activity was observed. In addition to the oscillations associated with the whistler wave, a train of ESWs with bipolar $E_\parallel$ is present. These bipolar electric fields correspond to structures with a net charge, such as electron phase space holes [*Ergun et al.*, 1998a, 1998b; *Cattell et al.*, 2005; *Graham et al.*, 2015].
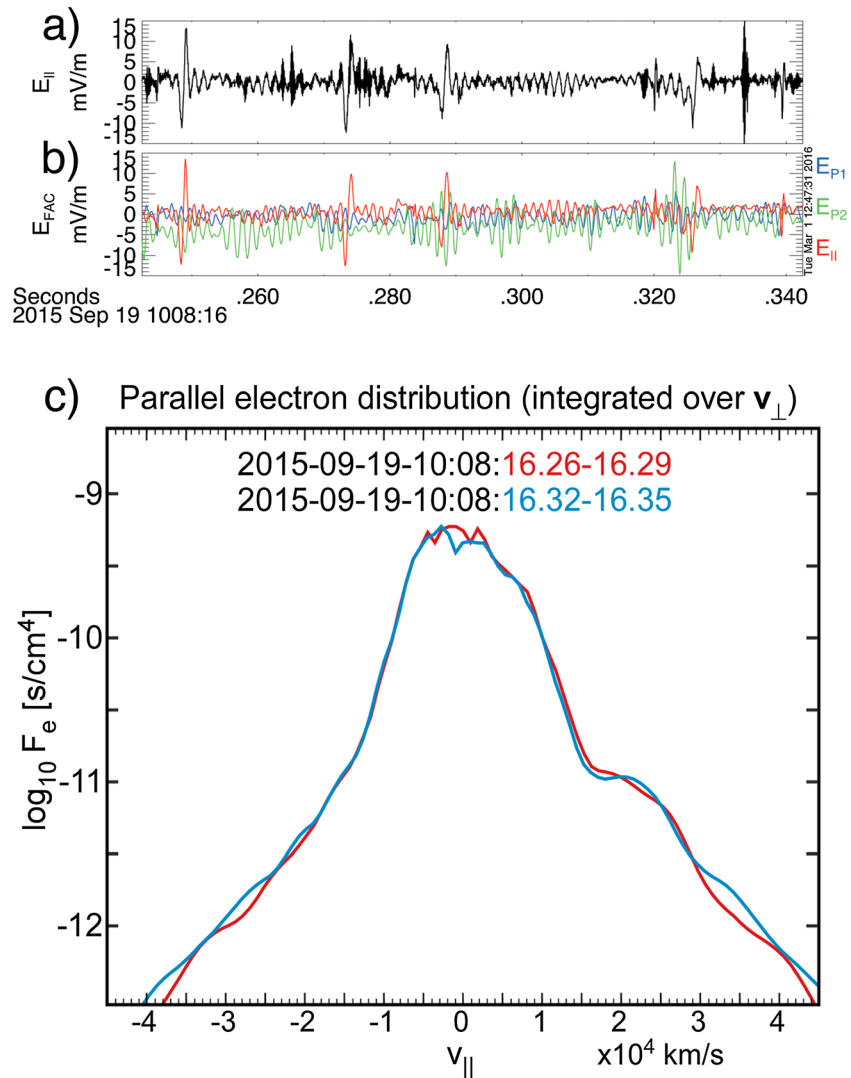
Figure 3. (a) $E_{||}$ at 65,536 S/s and (b) E_{FAC} at 8192 S/s for several bipolar parallel electric field signatures from Figure 2b. (c) Reduced FPI distributions, $F(v_{||})$, near the time ranges shown in Figure 2b.

Figure 3 shows the electric field time series surrounding several of these bipolar $E_{||}$ signatures with AC-coupled $E_{||}$ at 65,536 S/s (a) and the full DC-coupled vector in FAC at 8192 S/s (b). The electric field of the ESW has a polarity of negative-to-positive as it passes over the spacecraft. The electrostatic potential associated with the bipolar electric field suggests that the ESWs would be moving antiparallel to $\mathbf{B}_0$ if they were associated with an electron phase space hole with net positive charge, or parallel to $\mathbf{B}_0$ if they were associated with an electron enhancement with a net negative charge. As seen in Figure 3b, the ESWs are also embedded in the whistler mode wave, approximately in phase with the parallel component of the oscillation. This is the case for a majority of the ESWs seen in Figure 2e as well as several of the other wave trains observed between 10:06 and 10:09 UT.

Attempts to determine the speed of the ESWs using probe-to-probe interferometry were inconclusive for several reasons. First, the phase accuracy of the signals is approximately 4 μs, corresponding to a maximum measurable speed for coherent waves of 3750 km/s for the axial booms. This is significantly slower than both the electron thermal speed (~6000 km/s) and the predicted phase speed for the whistler waves (~25,000 km/s). For fitted solitary structures, the speed is limited by the data rate, which corresponds to a speed of ~122 km/s. The uncertainty in the phase delay was also exacerbated by a common mode oscillation in the spacecraft potential at the whistler frequency. The ESWs also were not clearly visible in the signal from the spin plane

booms. Regardless, one hypothesis is that since the ESWs appear to be in phase with the whistlers, they might correspond to a structure interacting with the waves. If this is the case, the bipolar fields are likely associated with an electron enhancement or ion hole, as the Poynting flux is mostly directed parallel to $\mathbf{B}_0$ (~20°), as opposed to antiparallel. Bipolar parallel electric fields at the magnetopause are typically assumed to be electron phase space holes, although *Cattell et al.* [2002] also identified some negative potential ESWs.

2.3. Reduced Electron Distribution Function

An advantage of using MMS to study nonlinear wave phenomena associated with magnetic reconnection is the high time cadence at which electron distribution functions can be measured (30 ms). Figure 3c shows the electron distribution, $F_e(v_{||})$, observed by FPI on MMS4 at two times between the vertical dashed lines in Figures 2e and 2f. $F_e(v_{||})$ was obtained by obtaining moments of the distribution for particle velocities perpendicular to $\mathbf{B}_0$. One important feature is the shoulder in the distribution near 20,000 km/s. Using the electric and magnetic field spectrum, we can determine the phase velocity, v_φ, of an electromagnetic wave with wave vector $\mathbf{k}$ perpendicular to $\mathbf{E}$, from equation (1),

$$v_\phi \sim |\delta\mathbf{E}|/|\delta\mathbf{B}|, \tag{1}$$

where $\delta\mathbf{E}$ and $\delta\mathbf{B}$ are oscillations in the electric and magnetic field. One way to evaluate equation (1) is spectrally. Particularly, we used electric and magnetic field power within four frequency bins of $f_{ce}/2$ (±30 Hz). Because equation (1) only applies to electromagnetic waves, we focus on periods when there are significant oscillations in $\mathbf{B}$ ($>10^{-4}$ nT^2/Hz). During these intervals, the measured phase velocity is between 17,000 and 23,000 km/s, which is in good agreement with the shoulder on the reduced distribution.

This measured reduced distribution function has been used to numerically solve the kinetic dispersion relation for the whistler anisotropy instability based on the equations from *Goldman and Newman* [1987]. Marginally stable whistler normal modes were found with frequencies near $f_{ce}/2$ (as in our observations) and phase velocity magnitudes near ± half the electron-Alfvén speed, which for this event was approximately 25,000 km/s. This is in good agreement with the observed phase speed using equation (1). If the observed whistlers are locally excited marginally stable whistlers they could be driven by spontaneous or nonlinear emission, which will be a subject of future study. The other possibility is that the whistler source region is remote. One hypothesis is that the waves could have been generated via perpendicular electron acceleration in the southward exhaust and then propagated northward back toward the X line.

Another question that still remains is what the shoulder in the distribution physically means. In simulations such shoulders have been associated with spiky bipolar fields arising from electron trapping [*Goldman et al.*, 2014; *Drake et al.*, 2015]. As seen in Figure 3c, sometimes the measured shoulder is just a decrease in the magnitude of the slope of $F_e(v_{||})$ (red trace), while other times, the slope goes from negative to positive (blue trace). In the latter case, this bump on the distribution drives Langmuir waves via a bump-on-tail instability with growth rate corresponding to approximately one *e*-folding per ms. The high-frequency parallel oscillations in the 65,536 S/s electric field data shown in Figure 3a lie near the electron plasma frequency (7–9 kHz). They are therefore likely Langmuir waves driven by the shoulder of the reduced distribution.

3. Summary and Conclusion

The present study shows observations by MMS of oblique whistler mode waves propagating near the separatrix of a reconnection exhaust. These waves are confined to the boundary layer and propagate at half the cyclotron frequency, suggesting they are likely to be locally generated via anisotropies in the electron distribution associated with the reconnection process, even though the measured ratio of $T_{eperp}/T_{e||}$ is very close to one. In addition, bipolar fields were found in phase with the whistler electric field oscillations. If these bipolar fields are propagating with the whistler waves parallel to the background field, they cannot be electron phase space holes, as are typically associated with bipolar $E_{||}$ signatures [*Ergun et al.*, 1998a, 1998b; *Matsumoto et al.*, 2003; *Cattell et al.*, 2002, 2005; *Graham et al.*, 2015].

Nonlinear wave-particle interaction is one area where magnetic reconnection is still poorly understood at the electron scale. The results of the present study suggest several topics for further investigation. First, because of the location of the whistler waves with respect to the separatrix, it is likely that the waves were generated locally at the magnetopause by the reconnection process. Additionally, if the waves were generated by

electron temperature anisotropy in the reconnection exhausts, it is still unclear why the waves fell on the magnetospheric, and not the magnetosheath, side of the separatrix. Further, because they are in phase with the parallel component of the whistler oscillations, it is likely the bipolar fields are related to the waves, but how they are generated requires further investigation. Because of the wave propagation direction, they may not be electron phase space holes, as have been observed during magnetopause reconnection in the past [*Graham et al.*, 2015]. Observations in the radiation belts by the Wind spacecraft have suggested that lower energy electron enhancements can occur in phase with whistler waves [e.g., *Kellogg et al.*, 2010], but this phenomenon has not been observed in association with magnetopause reconnection. Additionally, the trapping observed by *Kellogg et al.* [2010] included a distortion in the waveform over consecutive periods that were not observed in the present study. A further difference between this study and *Kellogg et al.* [2010] is that the bipolar fields are in the parallel direction, as opposed to the wave propagation direction. Additionally, whether or not the ESWs are related to the shoulder of the reduced distribution warrants further research. Finally, these waves could have an impact on energetic particles near the X line via cyclotron resonance, similar to how the waves can impact radiation belt particles [*Thorne*, 2010].

There are also differences and similarities between the case presented in the present study and past studies of waves and solitary structures related to reconnection. For example, *Tang et al.* [2013] observed whistler mode waves driven by electron temperature anisotropy that were propagating away from the X line, while the waves in the present event are propagating toward the X line, consistent with the statistical study by *Graham et al.* [2016]. One reason for these discrepancies could be that the present study, as well as *Graham et al.* [2016], was focused on the separatrix region, while *Tang et al.* [2013] showed an event near the electron diffusion region. Further, *Tang et al.* [2013] also observed ESWs, but they had no apparent phase relationship with the whistlers, and if the ESWs in the present study move with the whistlers, they will move at a different speed than those reported by *Drake et al.* [2003]. This is expected as *Graham et al.* [2015] suggested multiple instabilities could be responsible for different ESWs at varying speeds and spatiotemporal scales.

Modeling studies have suggested whistler waves and electrostatic solitary structures propagating toward the diffusion region could impact the reconnection electric field [e.g., *Lapenta* 2010; *Goldman et al.*, 2014]. The solitary structures in the present study, if they propagate at the wave phase speed, would have a length scale of ~30–45 km, which is on the order of a few electron skin depths (~6 km with an electron density of $0.75\,cm^{-3}$). This length scale is optimal for interacting with magnetic reconnection on the electron scale. Further work using both simulations and observations can help determine the role these waves play in mediating the reconnection process. With its high time resolution and 3-D measurement capabilities, the MMS mission is ideal for investigating these phenomena. The spacecraft has already encountered the magnetopause over 2000 times during the first dayside science phase and will continue to provide a wealth of data to study magnetic reconnection and plasma wave phenomena at the electron scale.

References

Birn, J., et al. (2001), Geospace Environmental Modeling (GEM) magnetic reconnection challenge, *J. Geophys. Res.*, *106*, 3715–3719, doi:10.1029/1999JA900449.

Burch, J. L., and J. F. Drake (2009), Reconnecting magnetic fields, *Am. Sci.*, *97*, 392.

Burch, J. L., T. E. Moore, R. B. Torbert, and B. L. Giles (2015), Magnetospheric Multiscale overview and science objectives, *Space Sci. Rev.*, doi:10.1007/s11214-015-0164-9.

Cattell, C., J. Crumley, J. Dombeck, J. Wygant, and F. S. Mozer (2002), Polar observations of solitary waves at the Earth's magnetopause, *Geophys. Res. Lett.*, *29*(5), 1065, doi:10.1029/2001GL014046.

Cattell, C., et al. (2005), Cluster observations of electron holes in association with magnetotail reconnection and comparison to simulations, *J. Geophys. Res.*, *110*, A01211, doi:10.1029/2004JA010519.

Che, H., J. F. Drake, M. Swisdak, and P. H. Yoon (2010), Electron holes and heating in the reconnection dissipation region, *Geophys. Res. Lett.*, *37*, L11105, doi:10.1029/2010GL043608.

Chen, Y., K. Fujimoto, C. Xiao, and H. Ji (2015), Plasma waves around separatrix in collisionless magnetic reconnection with weak guide field, *J. Geophys. Res. Space Physics*, *120*, 6309–6319, doi:10.1002/2015JA021267.

Deng, X. H., and H. Matsumoto (2001), Rapid magnetic reconnection in the Earth's magnetosphere mediated by whistler waves, *Nature*, *410*, 557–560.

Dungey, J. W. (1961), Interplanetary magnetic field and the auroral zones, *Phys. Rev. Lett.*, *6*, 47–48.

Drake, J. F., M. Swisdak, C. Cattell, M. A. Shay, B. N. Rogers, and A. Zeiler (2003), Formation of electron holes and particle energization during magnetic reconnection, *Science*, *299*, 5608, doi:10.1126/science.1080333.

Drake, J. F., O. V. Agapitov, and F. S. Mozer (2015), The development of a bursty precipitation front with intense localized parallel electric fields driven by whistler waves, *Geophys. Res. Lett.*, *42*, 2563–2570, doi:10.1002/2015GL063528.

Ergun, R. E., et al. (1998a), FAST satellite observations of large-amplitude solitary structures, *Geophys. Res. Lett.*, *25*, 2041–2044.

Ergun, R. E., C. W. Carlson, J. P. McFadden, F. S. Mozer, L. Muschietti, and I. Roth (1998b), Debye-scale plasma structures associated with magnetic-field-aligned electric fields, *Phys. Rev. Lett.*, *81*, 826.

Ergun, R. E., et al. (2014), The axial double probe and fields signal processing for the MMS Mission, *Space Sci. Rev.*, doi:10.1007/s11214-014-0115-x.

Eriksson, S., S. R. Elkington, T. D. Phan, S. M. Petrinec, H. Rème, M. W. Dunlop, M. Wiltberger, A. Balogh, R. E. Ergun, and M. André (2004), Global control of merging by the interplanetary magnetic field: Cluster observations of dawnside flank magnetopause reconnection, *J. Geophys. Res.*, *109*, A12203, doi:10.1029/2003JA010346.

Fujimoto, K., and R. D. Sydora (2008), Whistler waves associated with magnetic reconnection, *Geophys. Res. Lett.*, *35*, L19112, doi:10.1029/2008GL035201.

Goldman, M. V., and D. L. Newman (1987), Electromagnetic beam modes driven by anisotropic electron streams, *Phys. Rev. Lett.*, *58*, 1849.

Goldman, M. V., D. L. Newman, G. Lapenta, L. Andersson, J. T. Gosling, S. Eriksson, S. Markidis, J. P. Eastwood, and R. Ergun (2014), Cerenkov emission of quasiparallel whistlers by fast electron phase-space holes during magnetic reconnection, *Phys. Rev. Lett.*, *112*, 145002, doi:10.1103/PhysRevLett.112.145002.

Graham, D. B., Y. V. Khotyaintsev, A. Vaivads, and M. André (2015), Electrostatic solitary waves with distinct speeds associated with asymmetric reconnection, *Geophys. Res. Lett.*, *42*, 215–224, doi:10.1002/2014GL062538.

Graham, D. B., A. Vaivads, Y. V. Khotyaintsev, and M. André (2016), Whistler emission in the separatrix regions of asymmetric magnetic reconnection, *J. Geophys. Res. Space Physics*, *121*, 1934–1954, doi:10.1002/2015JA021239.

Hesse, M., T. Neukirch, K. Schindler, M. Kuznetsova, S. Zenitani (2011), The diffusion region in collisionless magnetic reconnection, *Space. Sci. Rev.*, *160*, doi:10.1007/s11214-010-9740-1.

Kellogg, P. J., C. A. Cattell, K. Goetz, S. J. Monson, and L. B. Wilson III (2010), Electron trapping and charge transport by large amplitude whistlers, *Geophys. Res. Lett.*, *37*, L20106, doi:10.1029/2010GL044845.

Khotyaintsev, Y. V., C. M. Cully, A. Vaivads, M. André, and C. J. Owen (2011), Plasma jet braking: Energy dissipation and nonadiabatic electrons, *Phys. Rev. Lett.*, *106*, 165001, doi:10.1103/PhysRevLett.106.165001.

Lapenta, G. (2010), Particle simulations of space weather, *J. Comput. Phys.*, *231*, 795.

Le Contel, O., et al. (2009), Quasi-parallel whistler mode waves observed by THEMIS during near-Earth dipolarizations, *Ann. Geophys.*, *27*, 2259–2275, doi:10.5194/angeo-27-2259-2009.

Le Contel, O., et al. (2014), The search-coil magnetometer for MMS, *Space Sci. Rev.*, doi:10.1007/s11214-014-0096-9.

Lindqvist, P.-A., et al. (2014), The spin-plane double probe electric field instrument for MMS, *Space Sci. Rev.*, doi:10.1007/s11214-014-0116-9.

Mandt, M. E., et al. (1994), Transition to whistler mediated magnetic reconnection, *Geophys. Res. Lett.*, *21*, 73–76.

Matsumoto, H., X. H. Deng, H. Kojima, and R. R. Anderson (2003), Observation of electrostatic solitary waves associated with reconnection on the dayside magnetopause boundary, *Geophys. Res. Lett.*, *30*(6), 1326, doi:10.1029/2002GL016319.

Mozer, F. S., P. L. Pritchett, J. Bonnell, D. Sundkvist, and M. T. Chang (2008), Observations and simulations of asymmetric magnetic field reconnection, *J. Geophys. Res.*, *113*, A00C03, doi:10.1029/2008JA013535.

Mozer, F. S., O. Agapitov, V. Krasnoselskikh, S. Lejosne, G. D. Reeves, and I. Roth (2014), Direct observation of radiation-belt electron acceleration from electron-volt energies to megavolts by nonlinear whistlers, *Phys. Rev. Lett.*, *113*, 035001, doi:10.1103/PhysRevLett.113.035001.

Øieroset, M., T. D. Phan, J. T. Gosling, M. Fujimoto, and V. Angelopoulos (2015), Electron and ion edges and the associated magnetic topology of the reconnecting magnetopause, *J. Geophys. Res. Space Physics*, *120*, 9294–9306, doi:10.1002/2015JA021580.

Omura, Y., M. Hikishima, Y. Katoh, D. Summers, and S. Yagitani (2009), Nonlinear mechanisms of lower-band and upper-band VLF chorus emissions in the magnetosphere, *J. Geophys. Res.*, *114*, A07217, doi:10.1029/2009JA014206.

Russell, C. T., et al. (2014), The magnetospheric multiscale magnetometers, *Space Sci. Rev.*, doi:10.1007/s11214-014-0057-3.

Samson, J. C., and J. V. Olson (1980), Some comments on the descriptions of the polarization states of waves, *Geophys. J. R. Astron. Soc.*, *61*, 115–129.

Tang, X., C. Cattell, J. Dombeck, L. Dai, L. B. Wilson III, A. Breneman, and A. Hupach (2013), THEMIS observations of the magnetopause electron diffusion region: Large amplitude waves and heated electrons, *Geophys. Res. Lett.*, *40*, 2884–2890, doi:10.1002/grl.50565.

Thorne, R. M. (2010), Radiation belt dynamics: The importance of wave-particle interactions, *Geophys. Res. Lett.*, *37*, L22107, doi:10.1029/2010GL044990.

Torbert, R. B., et al (2014), The electron drift instrument for MMS, *Space Sci. Rev.*, doi:10.1007/s11214-015-0182-7.

Trattner, K. J., et al. (2016), The response time of the magnetopause reconnection location to changes in the solar wind: MMS case study, *Geophys. Res. Lett.*, *43*, 4673–4682, doi:10.1002/2016GL068554.

Viberg, H., Y. V. Khotyaintsev, A. Vaivads, M. André, H. S. Fu, and N. Cornilleau-Wehrlin (2014), Whistler mode waves at magnetotail dipolarization fronts, *J. Geophys. Res. Space Physics*, *119*, 2605–2611, doi:10.1002/2014JA019892.

Wang, R., et al. (2014), Observation of double layer in the separatrix region during magnetic reconnection, *Geophys. Res. Lett.*, *41*, 4851–4858, doi:10.1002/2014GL061157.

Wei, X. H., J. B. Cao, G. C. Zhou, O. Santolík, H. Rème, I. Dandouras, N. Cornilleau-Wehrlin, E. Lucek, C. M. Carr, and A. Fazakerley (2007), Cluster observations of waves in the whistler frequency range associated with magnetic reconnection in the Earth's magnetotail, *J. Geophys. Res.*, *112*, A10225, doi:10.1029/2006JA011771.